Investigation of Nonisothermal Crystallization of Hydroxyapatite/Ethylene-Vinyl Acetate (HA/EVA) Composite

Yanying Wang,[1] Li Zhang,[2] Song Zhou,[2] Di Huang,[2] Yos Morsi,[3] Shibo Gao,[2] Mei Gong,[2] Yubao Li[2]

[1]*China Department of Chemistry, Sichuan University, 610064 Chengdu, China*
[2]*Research Center for Nano-Biomaterials, Analytical and Testing Center, Sichuan University, Chengdu 610064, China*
[3]*Faculty of Engineering and Industrial Sciences, Swinburne University of Technology, Hawthorn, VIC, 3122, Australia*

Received 2 September 2010; accepted 3 January 2011
DOI 10.1002/app.34091
Published online 23 May 2011 in Wiley Online Library (wileyonlinelibrary.com).

ABSTRACT: Hydroxyapatite/ethylene-vinyl acetate (HA/EVA) composites were prepared by injection molding and characterized by X-ray diffraction (XRD) and attenuated total multiple reflection infrared (ATR-IR) spectroscopy. The nonisothermal crystallization behavior of HA/EVA composites at different cooling rates and with different HA content were examined by differential scanning calorimetry (DSC). The results exhibit the occurrence of interaction between HA and EVA, and the HA particles in EVA matrix act as effective nucleation agent. The addition of HA influences the mechanism of nucleation and growth of EVA crystallites. HA particles, as nucleus, are efficient to promote EVA crystallization at early stage but prevent EVA crystal growth in the late stage. The EVA crystallization in the composite is mainly through heterogeneous nucleation. © 2011 Wiley Periodicals, Inc. J Appl Polym Sci 122: 1412–1419, 2011

Key words: hydroxyapatite; ethylene-vinyl acetate; composite; nonisothermal crystallization; DSC

INTRODUCTION

In recent years, polymer–inorganic composites for biomedical applications have attracted great attention in the literature. Hydroxyapatite (HA, $Ca_{10}(PO_4)_6(OH)_2$) is well recognized as a promising inorganic component in the polymer matrix,[1–6] due to its excellent biocompatibility and bioactivity, and it has been widely used in orthopedic, dental, and maxillofacial fields.[7–9] However, the clinical application of HA bioceramics is limited by its brittleness, especially in load-bearing situation.[10,11] Ethylene vinyl acetate (EVA) copolymer has good flexibility and toughness, and has been used in food and drug industry.[12–15] Accordingly, a novel composite with EVA as the matrix and HA particles as the filler has been designed for cranioplasty applications.[16,17] This composite is expected to be malleable and easy to sculpt precisely according to the defect based on the plasticity of EVA. The existence of HA particles in EVA matrix is helpful to improve the strength of the composite and to endow the composite with bone-bonding bioactivity.

It is known that the physical and mechanical properties of polymers depend primarily on the morphology, crystalline structure, and degree of crystallization. The behavior of thermoplastic semicrystalline polymers during nonisothermal crystallization is critical for real industrial processing applications.[18] Li et al. have studied the influence of carbon nanotubes on the crystallization of EVA and found the high nucleation ability of carbon nanotubes in EVA.[19] Shi et al. researched the influence of VAC content on the crystallization of EVA.[20] Nonisothermal crystallization kinetics of PP/EVA, LDPE/EVA, and LLDPE/EVA blends were reported by Goodarzi, Jin, Moly and their coworkers, respectively.[21–24] Although there are a few papers dealing with the HA/EVA composite, the effect of HA filler on crystallization behavior of HA/EVA is still unclear. In this study, HA/EVA composites were prepared by using injection-molding method, the nonisothermal crystallization behavior of HA/EVA was investigated and nonisothermal crystallization kinetic equations were used for the analysis.

Correspondence to: Yubao Li (nic7504@scu.edu.cn).
Contract grant sponsor: 863 Funds; contract grant number: 2007AA03Z328766.
Contract grant sponsor: China 973 Funds; contract grant number: 2007CB936102.

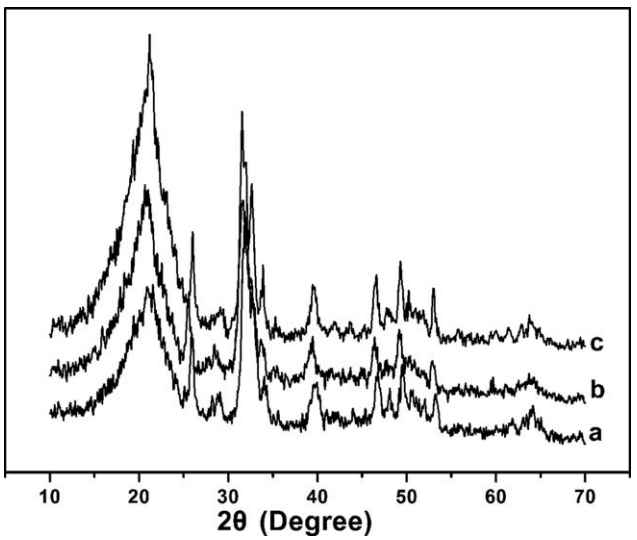

Figure 1 XRD patterns of HA/EVA composites containing 30 wt % HA (a), 20 wt % HA (b), and 10 wt % HA (c).

EXPERIMENTAL

EVA copolymer was from Exxon Mobil. ModelUL7710, USA with a vinyl acetate (VA) content of 28 wt %. HA powders were prepared in our lab[25] with an average particle size less than 200 μm. EVA raw material and HA particles were dried in a vacuum chamber at 60°C for 24 h. Pure EVA and HA/EVA composites with different HA content were extruded separately in a corotating twin-screw extruder (Model TSSJ, Φ30 mm, $L : D = 36 : 1$, Chengdu Keqiang, China). A temperature ranging from 90 to 140°C with a screw rotational speed of 200 rpm was applied to melt the EVA raw material and to ensure a good mixing of EVA with HA particles. The extrudates were cooled in distilled water and pelletized. Then the pelletized extrudates were dried at 60°C for 24 h in vacuum chamber and molded into standard mechanical testing specimens by injection-molding machine (Model FT-90, Shenda, China) at a temperature from 90 to 110°C.

Fourier transform infrared absorption spectroscopy (FTIR, Nicolet Perkin–Elmer) was used to determine the interactions between inorganic phase and polymer phase. The FTIR spectrum of HA was obtained over a wavenumber range of 4000–400 cm^{-1} with 4 cm^{-1} resolution using an infrared spectrometer with a KBr/sample ratio of 100/1. The attenuated total multiple reflection technique (ATR-IR) was used for EVA and HA/EVA analysis. The ATR-IR spectra of EVA and HA/EVA composites were obtained over a wavenumber range of 4000–600 cm^{-1} with 4 cm^{-1} resolution. The samples were cut into 1.5 × 1.1 cm^2 pieces with 0.20-mm thick. X-ray diffraction (XRD) was used to detect the phase composition and crystallization behavior. The XRD data were collected on a D/M-rA diffractometer (DX-2600, Dandong China) with Cu Kα radiation ($\lambda = 0.1548$ nm) and operated at 40 kV and 100 mA. The 2θ scanning range was from 10° to 70° at a scanning speed of 0.05° per second.

The crystallization behaviors of EVA and HA/EVA composites were determined using a differential scanning calorimeter (DSC-204 Phoenix, Netzsch, Germany) in a nitrogen atmosphere. The heat history of the samples was eliminated and 6 mg of each sample was used in the analysis. The samples were scanned at a cooling rate of 2.5, 5, 10, and 20°C min^{-1}, respectively.

RESULTS AND DISCUSSION

XRD characteristics

Figure 1 shows the XRD patterns of HA/EVA composites with HA content of 10–30 wt %. It can be seen that the peaks at $2\theta = 25.94°$ (002), 31.81° (211), 39.84° (310), 46.63° (222), 49.70° (213), and 53.19° (004) match well with the diffraction peaks of stoichiometric hydroxyapatite (JCPDS card No.09-0432). The peak intensity of EVA at $2\theta = 21.25°$ decreases with the increase of HA content, indicating that the amorphous region of EVA has enlarged. The interfacial bonding between HA particles and EVA matrix may disturb the EVA crystallization process by decreasing chain orders, thus decrease the crystal intensity of EVA polymer.

ATR-IR analysis

Figure 2 shows the IR spectra of HA, EVA, and EVA/HA 30 wt % composites. In Figure 2(a), the FT-IR absorption bands of OH (3571 cm^{-1}), H_2O

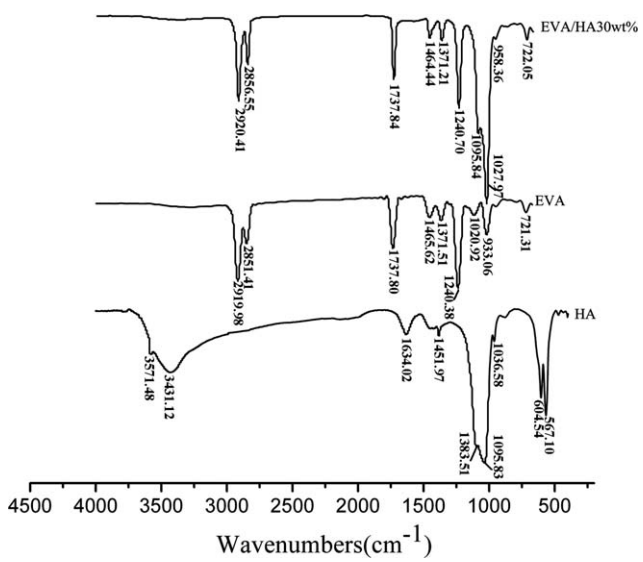

Figure 2 FT-IR spectrum of HA (a) and ATR-IR spectra of EVA (b), 30 wt % HA/EVA (c).

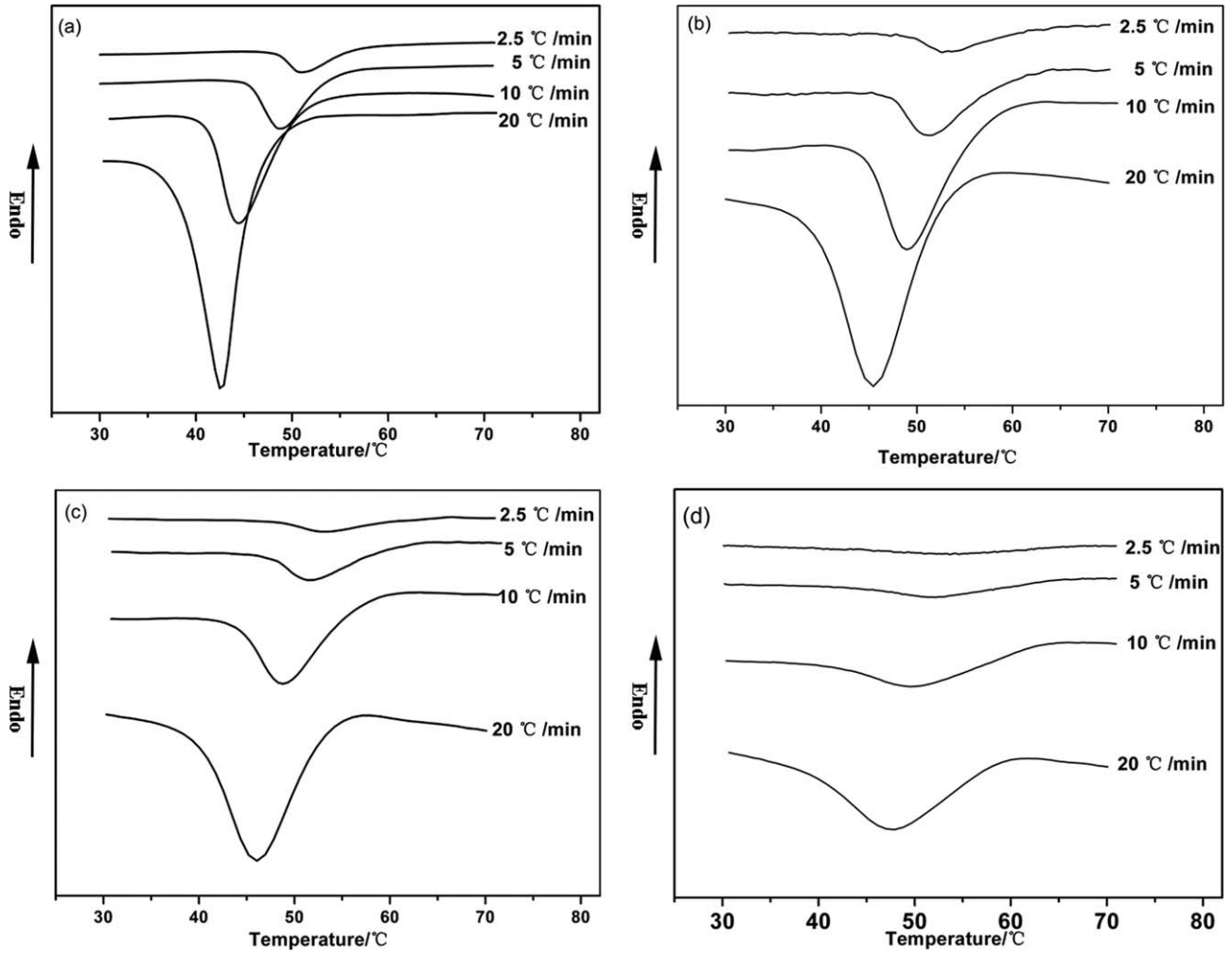

Figure 3 DSC thermograms of nonisothermal crystallization at different cooling rates, EVA (a), 10 wt % HA/EVA (b), 20 wt % HA/EVA (c), and 30 wt % HA/EVA (d).

(3431 and 1634 cm^{-1}) and PO_4^{3-} (1095, 1036, and 604 cm^{-1}) belonging to HA crystals are all present. The ATR-IR spectra of pure EVA in Figure 2(b) shows that the typical absorption bands of vinyl acetate group appear at 1737, 1240, and 1020 cm^{-1}, while the absorption bands ascribing to ethylene group are present at 2919, 2851, 1465, 1371, and 721 cm^{-1}. After forming the composite, some bands of the EVA polar groups shift apparently, e.g., the bands of 1240.38 and 1020.92 cm^{-1} in Figure 2(b) move respectively, to 1240.70 and 1027.97 cm^{-1} in Figure 2(c). The stretching absorption peak at 3571 cm^{-1} of the hydroxyl group can not be observed in the composites. The bands shift indicates that the hydroxyl groups on the surface of HA crystals may interact with the polar vinyl acetate groups of EVA. As the formation of hydrogen bond, the bonding of HA filler and EVA polymer leads to affinity and stiffness of composites. Based on the findings of IR and XRD analyses, it can be deduced that molecular interaction is present between HA and EVA in the composite, which may greatly affect the crystallization behavior and properties of the composite.

Nonisothermal crystallization behavior

The DSC thermograms of nonisothermal crystallization of EVA and HA/EVA composites at different cooling rates (2.5, 5, 10, and 20°C min^{-1}) are shown in Figure 3(a–d). The exothermal curves of heat flow as a function of temperature were recorded to analyze the nonisothermal crystallization process. The crystallinities of these samples were determined from the heat of crystallization. The curves indicate that the crystallization peak temperature decreases with increasing cooling rates. At a relative low cooling rate, there is sufficient time to activate nuclei; therefore, the crystallization can occur at a higher temperature.

Figure 4 gives the crystallization peak temperature versus cooling rate for EVA and HA/EVA composite. It can be seen that the peak crystallization

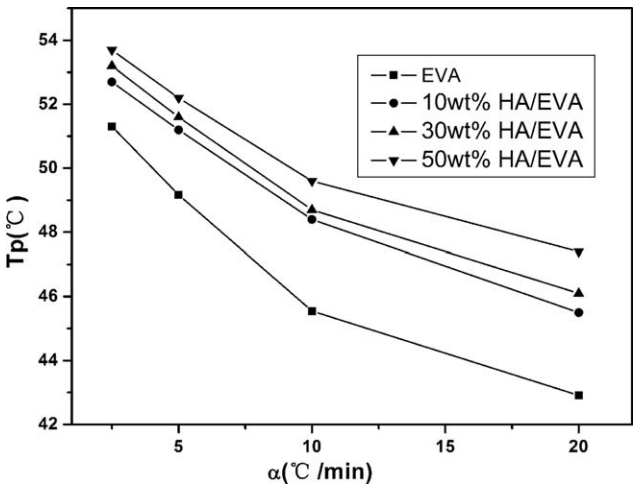

Figure 4 Crystallization peak temperature versus cooling rate (α) for EVA and HA/EVA.

temperature (T_p) of all composites is higher than that of EVA at different cooling rates, and the more the HA content is in the composite, the higher is the peak crystallization temperature. This phenomenon can be explained by the heterogeneous nucleation effect of HA particles on EVA macromolecular segments which can attach easily to the surface of HA crystals by interaction. This will make the crystallization of EVA occur at a higher crystallization temperature.

Nonisothermal crystallization kinetics

To analyze the nonisothermal crystallization process, the crystallization kinetics of HA/EVA composites with 10–30 wt % HA content is studied. From dynamic crystallization experiments, the data from the crystallization exotherms as a function of temperature, i.e., the dH/dT, can be determined for each cooling rate. The relative degree of crystallinity as a function of temperature, X_T, can be calculated according to eq. (1).[26]:

$$X_T = \frac{\int_{T_0}^{T}(dH/dT)dT}{\int_{T_0}^{T\infty}(dH/dT)dT} \quad (1)$$

where T_0 and T_∞ are the temperatures at which crystallization starts and ends. dH/dT is the heat flow rate. The development of relative degree of crystallinity X_T as a function of temperature T for the composites at different cooling rates is shown in Figure 5. The plots of $1 - X_T$ versus T for EVA and HA/EVA composites are similar and all these curves have the same sigmoidal shape, implying that only a lag effect of cooling rate on crystallization is observed. In the nonisothermal crystallization, the time t has the following relation with the temperature T:

$$t = (To - T)/\alpha \quad (2)$$

where T is the temperature at time t, T_0 is the onset crystallization temperature, and α is the cooling rate. According to eq. (2) the value of T on the X-axis can be transferred into the crystallization time (t). The calculated t data show that the higher the cooling rate, the shorter the time for completing crystallization.

Various methods have been suggested to study the nonisothermal crystallization of polymers.[27–34] Generally isothermal crystallization kinetics is explained by Avrami equation but eq. (3),[35–37] was also adopted as an alternative approach, according to which the equivalent time-dependent crystallinity X_T can be expressed as,

$$1 - X_T = \exp(-Z_t t^n) \quad (3)$$

where X_T is the relative crystallinity degree, n is the Avrami exponent, t is the time, and Z_T is the growth rate constant. Here, n represents the nucleation mechanism and growth dimension. Equation (3) can be integrated in its double logarithmic form:

$$\ln[-\ln(1 - X_T)] = \ln Z_t + n \ln t \quad (4)$$

By fitting the experimental data in eq. (4) the value of n can be obtained from the slope of the plots of ln[- ln(1 - X_T)] versus ln$t$ for each cooling rate in Figure 6. The experimental data are represented by the Avrami equation for the early stage of crystallization only. The Avrami equation is not applicable in the late stage where secondary nucleation takes place. The experimental data based on the early stage of crystallization are often used for analysis with linear fitting. It should be noticed that in nonisothermal crystallization, Z_t and n do not have the same physical significance as in isothermal crystallization because the temperature changes constantly under nonisothermal crystallization. Since the rate of nonisothermal crystallization depends on the cooling rate, Jeziorny[28] suggested that the rate parameter Z_t should be corrected for the influence of cooling rate α of the polymer. The parameters characterizing the kinetics of nonisothermal crystallization are given as follows:

$$\ln Z_c = \ln Z_t/\alpha \quad (5)$$

The nonisothermal crystallization parameters n and Z_c fitting to the kinetics are listed in Table I. The Avrami exponent is known to be influenced by the molecular weight, nucleation type, and

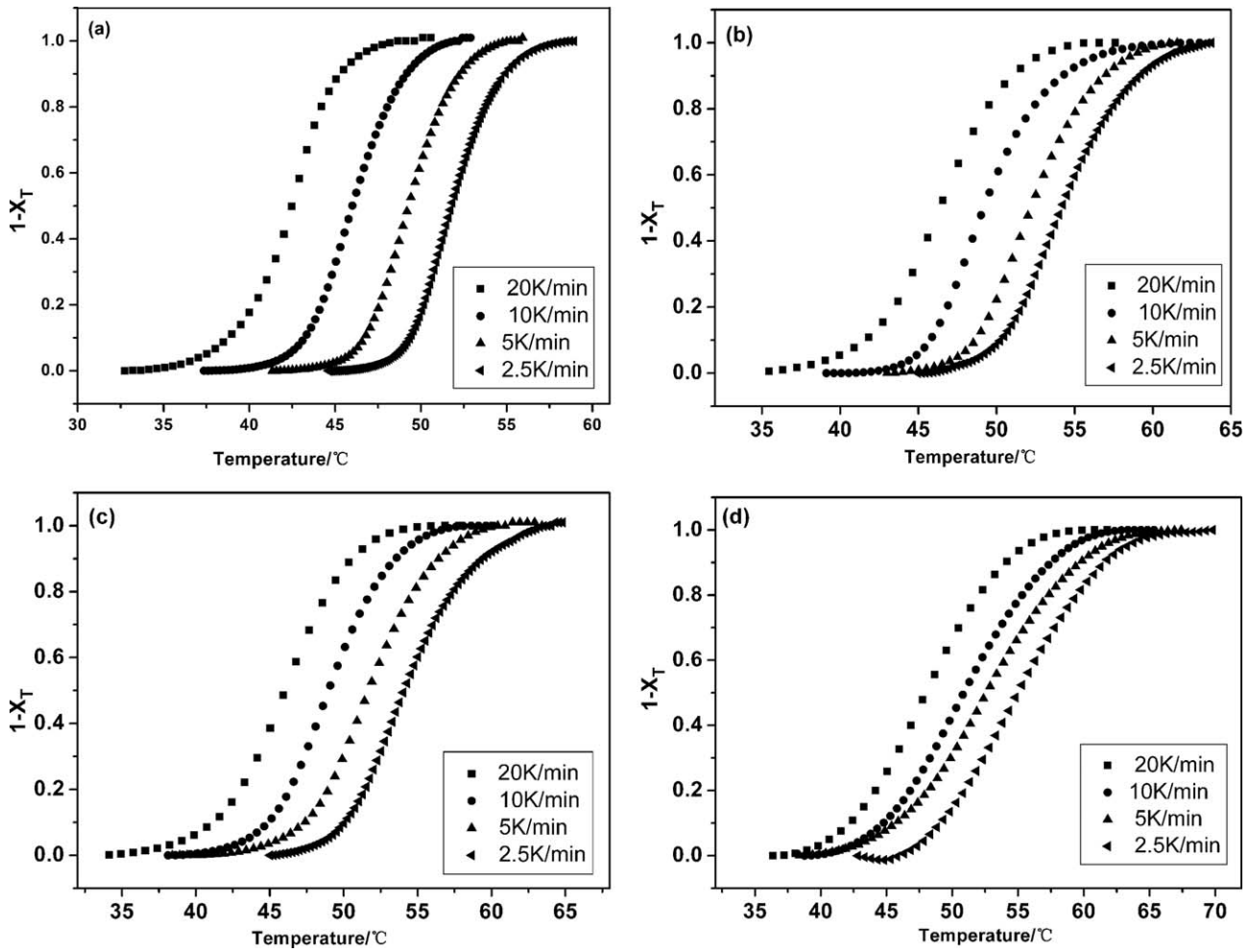

Figure 5 Plot of 1 - X_T as a function of temperature for EVA (a), 10 wt % HA/EVA (b), 20 wt % HA/EVA (c), and 30 wt % HA/EVA (d) crystallized nonisothermally at different cooling rates.

secondary crystallization, and in general, not much affected by the temperature variation. The Avrami exponent of EVA is close to 4, indicating that spherulite growth likely occurs with homogeneous nucleation. With the increase of HA content, the values of n for HA/EVA composites become lower than that of EVA at the same cooling rate. For the composites, the Avrami exponent is found to be between 3 and 4, suggesting that the nucleated process gradually changes from homogeneous nucleation to heterogeneous nucleation. It should be noted that HA crystals act as nuclei for the initial nucleation of EVA. The Jeziorny crystallization rate constant Z_c is also affected by the content of HA, showing an increased trend with HA content. The results indicate that the EVA crystallization in the composite is mainly through heterogeneous nucleation, followed by three-dimensional and diffusion-controlled growth.

Another approach suggested by Mo and coworkers[33,34] is to combine the Avrami equation with the Ozawa equation to study the nonisothermal crystallization. Their corresponding kinetic equation is used here to study the nonisothermal crystallization behavior of the HA/EVA composites. As the degree of crystallinity is related to the cooling rate α and the crystallization time t (or temperature T), the relation between α and t can be defined for a given degree of crystallinity by:

$$\ln Z_t + \ln t = K(T) - m \ln \alpha \tag{6}$$

$$\ln \alpha = \ln F(T) - a \ln t \tag{7}$$

where the kinetic parameter, $F(T) = [K(T)/Z_t]^{1/m}$. $F(T)$ has a definite physical and practical meaning, the smaller the value of $F(T)$, the higher the crystallization rate becomes. The Mo exponent a is the ratio of the Avrami exponent n to the Ozawa exponent m, that is, $a = n/m$. Indeed, according to eq. (7) and at a given degree of crystallinity, plotting lnα versus ln$t$ should yield a linear relationship. The kinetic

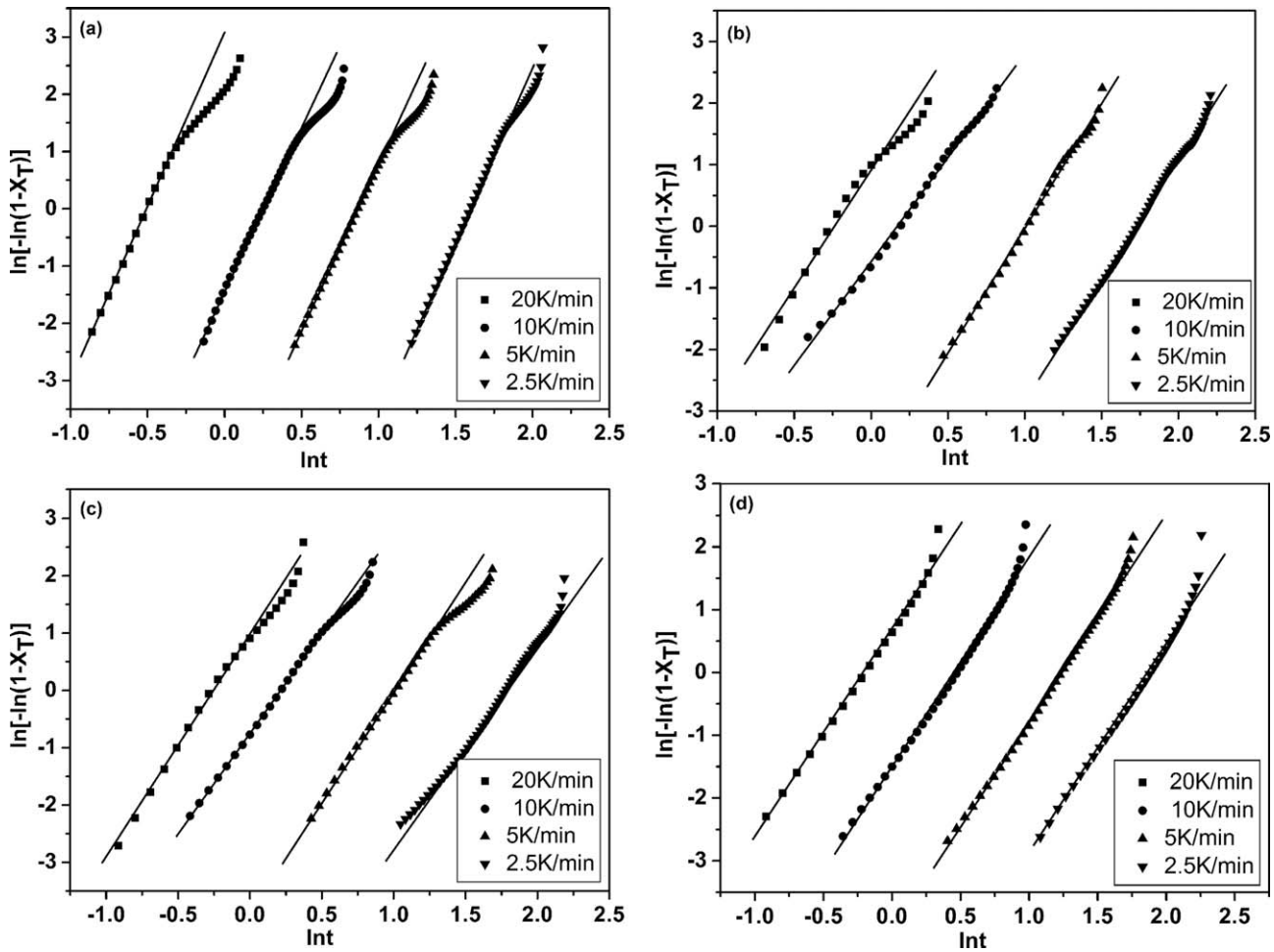

Figure 6 Plot of ln[- ln(1 - X_T)] as a function of ln$t$ for EVA (a), 10 wt % HA/EVA (b), 20 wt % HA/EVA (c), and 30 wt % HA/EVA (d).

parameters $F(T)$ and a are determined from the intercept and slope of the lines, respectively. Plots of lnα versus ln$t$ at various degree of crystallinity for EVA and HA/EVA composites are presented in Figure 7. As it can be seen from the figures, good linearity is observed which verifies the advantage of the combined approach applied here.

TABLE I
Nonisothermal Crystallization Parameters Obtained by Avrami (n) and Jeziorny (Zc) Methods

Sample	α (°C min^{-1})	Zc	n
EVA	2.5	0.03	4.50
	5	0.37	4.48
	10	0.87	4.33
	20	1.16	4.02
10 wt % HA/EVA	2.5	0.06	3.95
	5	0.44	4.04
	10	0.94	3.67
	20	1.04	3.56
20 wt % HA/EVA	2.5	0.07	3.58
	5	0.47	3.58
	10	0.95	3.51
	20	1.05	3.55
30 wt % HA/EVA	2.5	0.08	3.32
	5	0.49	3.32
	10	0.96	3.33
	20	1.03	3.33

The calculated values for a and $F(T)$ are listed in Table II. The value of a varies from 1.00 to 1.02 for pure EVA and from 0.96 to 1.02 for HA/EVA composites. On the whole, the a values of EVA are slightly higher than those of its composites at the same relative degree of crystallinity (X_T). Comparing with the pure EVA, the values of $F(T)$ systematically decrease with increase of X_T before 40% and increase with X_T after 60% in 10 and 20 wt %HA/EVA composites. And the value of $F(T)$ decreases with increase of X_T at 20% and increases with X_T after 40% in 30 wt % HA/EVA composite. From the $F(T)$ data when X_T is 20%, it can be deduced that incorporation of HA particles as nucleus is beneficial for the promotion of EVA crystallization at the early stage. However more HA content may also reduce the mobility of crystallizable EVA chain segments and inhibit the EVA crystal growth in the late stage, as for the composite of 30 wt %HA/EVA.

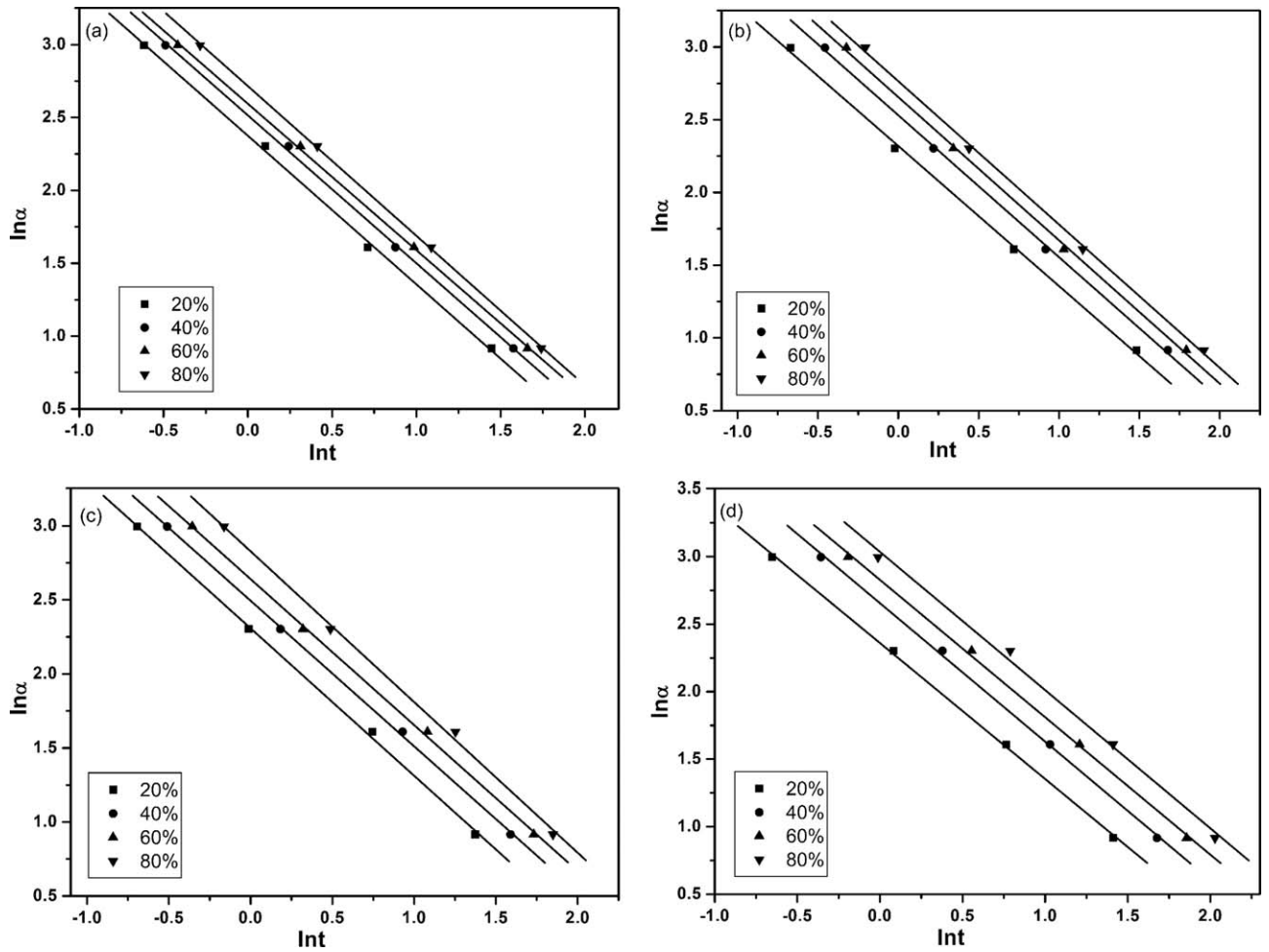

Figure 7 Plots of lnα as a function of ln*t* for EVA (a), 10 wt % HA/EVA (b), 20 wt % HA/EVA (c), and 30 wt % HA/EVA (d).

CONCLUSIONS

In this study, HA-filled EVA composites were prepared by injection molding. The XRD and IR analyses indicate the existence of interaction between HA and EVA. Based on nonisothermal crystallization kinetics, the Avrami model modified by Jeziorny and Mo can successfully describe the nonisothermal crystallization process of EVA in HA/EVA composite. Different kinetic parameters determined from these models prove that HA filler is efficient to promote EVA crystallization at early stage by its nucleation, but more HA content in the composite may also reduce the mobility of crystallizable EVA chain segments and inhibit the EVA crystal growth in the late stage of crystallization. Consequently, the type of nucleation and growth of EVA crystallites can be markedly changed by the presence of HA particles.

TABLE II
Kinetic Parameters for EVA and HA/EVA Composites at Different Relative Degrees of Crystallinity

Sample	X_T (%)	*a*	*F*(*T*)
EVA	20	1.02	10.75
	40	1.01	12.36
	60	1.00	13.39
	80	1.02	15.26
10 wt % HA/EVA	20	0.96	10.16
	40	0.97	12.19
	60	0.98	14.23
	80	0.98	15.87
20 wt % HA/EVA	20	1.00	10.05
	40	0.98	12.11
	60	0.99	14.02
	80	1.01	16.91
30 wt % HA/EVA	20	1.01	10.59
	40	1.02	14.23
	60	1.02	16.91
	80	1.02	20.81

References

1. Bonfield, W.; Wang, M.; Tanner, K. E. Acta Mater 1998, 46, 2509.
2. Ramakrishna, S.; Mayer, J.; Wintermantel, E.; Kam, L. W. Compos Sci Technol 2000, 61, 1189.
3. Rizzi, S. C.; Heath, D. T.; Coombes, A. G. A.; Bock, N.; Textor, M.; Downes, S. J Biomed Mater Res 2001, 55, 475.

4. Wang, X. J.; Li, Y. B.; Wei, J.; Grood, D. K. Biomaterials 2002, 23, 4787.
5. Wang, M.; Bonfield, W. Biomaterials 2001, 22, 1311.
6. Liao, J. G.; Zhang, L.; Zuo, Y.; Wang, H. N.; Li, J. D.; Zou, Q.; Li, Y. B. J Biomater Appl 2009, 24, 31.
7. Ducheyne, P. J Biomed Mater Res Appl Biomater 1987, 21, 219.
8. Heise, U.; Osborn, J. F.; Duwe, F. Int Orthop 1990, 14, 329.
9. Hench, L. L.; Polak, J. M. Science 2002, 295, 1014.
10. Ruys, A. J.; Wei, M.; Soreell, C. C.; Dickson, M. R.; Brandwood, A.; Milthorpe, B. K. Biomaterials 1995, 16, 409.
11. Lu, L.; Mikos, A. G. MRS Bull 1996, 21, 28.
12. Sam, A. P. J Control Release 1992, 22, 35.
13. Langer, R.; Brem, H.; Tapper, D. J Biomed Mater Res 1981, 15, 167.
14. Niemi, S. M.; Fox, J. G.; Brown, L. R.; Langer, R. Lab Sci 1985, 35, 609.
15. Shastri, P. V. Contraception 2002, 65, 9.
16. Velayudhan, S.; Ramesh, P.; Varma, H. K.; Friedrich, K. Mater Chem Phys 2005, 89, 454.
17. Velayudhan, S.; Ramesh, P.; Sunny, M. C.; Varma, H. K. Mater Lett 2000, 46, 142.
18. Wunderlich, B. Macromolecular Physics; Academic Press: New York, 1973.
19. Li, S. N.; Li, Z. M.; Yang, M. B.; Hu, Z. Q.; Xu, X. B.; Huang, R. Mater Lett 2004, 58, 3967.
20. Shi, X. M.; Zhang, J.; Jin, J.; Chen, S. J. Express Polym Lett 2008, 2, 623.
21. Goodarzi, V.; Jafari, S.-H.; Khonakdar, H. A.; Monemian, S. A.; Hässler, R.; Jehnichen, D. J Polym Sci B Polym Phys 2009, 47, 674.
22. Jin, J.; Chen, S. J.; Zhang, J. Express Polym Lett 2010, 4, 141.
23. Moly, K. A.; Radusch, H. J.; Androsh, R.; Bhagawan, S. S.; Thomas, S. Eur Polym Mater 2005, 6, 1410.
24. Jin, J.; Chen, S. J.; Zhang, J. Express Polym Lett 2010, 4, 141.
25. Li, Y. B.; Grood, D. K.; Dewijn, J.; Klein, C. P. A. T.; Meer, S. V. D. J Mater Sci Mater Med 1994, 5, 3261.
26. Cebe, P.; Hong, S. D. Polym 1986, 27, 1183.
27. Ziabicki, A. Appl Polym Sym 1967, 6, 1.
28. Jeziorny, A. Polymer 1978, 19, 1142.
29. Patel, R. M.; Spruiell, J. E. Polym Eng Sci 1991, 31, 730.
30. Nakamura, K.; Watanabe, T.; Katayama, K.; Amano, K. J Appl Polym Sci 1972, 16, 1077.
31. Chan, T. W.; Shyu, G. D.; Isayev, A. I. Rubber Chem Technol 1993, 64, 849.
32. Sifleet, W. L.; Dinos, N.; Collier, J. R. Polym Eng Sci 1973, 13, 10.
33. Liu, J. P.; Mo, Z. S.; Qi, Y. C.; Zhang, H. F.; Chen, D. L. Acta Polym Sinica 1993, 1, 1.
34. Cebe, P. Polym Compos 1988, 9, 271.
35. Avrami, M. J Chem Phys 1939, 7, 1103.
36. Avrami, M. J Chem Phys 1940, 8, 212.
37. Wunderlich, B. Macromolecular Physics; Academic Press: New York, 1976.